Particle
& Particle Systems Characterization
www.particle-journal.com

Materials Views
www.MaterialsViews.com

Self-Oriented Nanojoining of Silver Nanowires via Surface Selective Activation

Peng Peng, Lei Liu, Adrian P. Gerlich, Anming Hu,* and Y. Norman Zhou**

With the extensive study of nanoelectronic devices and nanoelectromechanical systems (NEMS), nanointerconnections have become a necessity for extremely dense logic circuits.[1] Bottom-up assembly of metallic one-dimensional (1D) nanostructures is one of the most efficient methods to construct nanocircuits. Silver nanowires (Ag NW), one of the nanostructured materials, have attracted considerable interest because of their excellent electrical conductivity and mechanical properties. Although some methods such as soldering,[2–4] voltage and/or current excitation,[5–8] thermal sintering,[9,10] electron beam irradiation,[11–13] laser irradiation,[14,15] and plasmon interactions[16] have been successfully used to create nanojunctions, local heating of some form is a general feature of these nanoscale welding techniques. As the size range transitions to the nanoscale, an increasing surface to volume ratio[17] in the nanostructured materials enhances their sensitivity to heat. However, local heating is often detrimental to the properties of the base material or damage the underlying substructures. In addition it is difficult to precisely control the application of heat at the nanoscale. Due to these limitations, the joining of Ag NWs without heating is essential to engineer nanocircuits and would be considered an attractive technical solution for the electronic industry. Lu et al.[1] have demonstrated that the cold welding of nanowires is possible by simply contacting two gold nanowires, such that surface-atom diffusion and oriented-attachment leads to successful welding. In the case of Ag NWs with highly oriented crystal structure produced by synthesis from a polyol solution,[18] this joining mechanism is generally precluded due to the layer of residual polyvinylpyrrolidone (PVP) that remains on the surface of the nanowires, thus the spontaneous cold welding mechanism has not been reported for Ag NWs. However, if the protective organic layer is removed then one could readily achieve this oriented attachment and promote cold welding of Ag NWs if the surface is activated. This is mainly driven by the high surface to volume ratio of the NW ends, which enhances atom diffusion as shown in the simulated results of Pereira and da Silva.[19] The prior work suggested that discontinuous Ag NW networks can be formed at room-temperature by changing the surface condition of Ag NWs via different washing procedures.[20]

Here, nanojunctions between individual Ag NWs with five-fold symmetry are created by following the surface activation. Through high-resolution transmission electron microscopy (HRTEM) and selected area electron diffraction (SAED), the phase relationship and joint formation mechanism between Ag NWs are investigated. The phase orientation between the two Ag NWs in the joint is analytically studied and explained based on the crystallography of the oriented nanowires. These self-oriented welded regions reveal that a similar crystal orientation is maintained between the nanowires, and the diffusion along the boundary contributes to the nanojunction formation. Those oriented joints could exhibit same strength and electrical conductivity as the rest of the nanowires.[1] Further, these monocrystalline V-shaped or zig-zag silver prisms terminated by twin boundaries and free surfaces may be a novel structure for investigating the transport of electrons, light, and vibrations in curved Ag NWs.

Ag NWs were prepared in a seeded polyol solution with PVP as a structure directing reagent using a method modified from the literature.[20–22] The as-synthesized Ag NWs are 8–16 μm long as shown in the optical microscopy image in **Figure 1**a with an average diameter of 100 nm. The NW end facets were selectively activated by simply washing with deionized (DI) water, then the considerable amount of NWs were end-to-end joined as shown in Figure 1b. It is interesting to note that most of them show V-shaped or zig-zag structures with approximately 2 to 4 straight NW segments joined at similar angles. When the angles of the joints are measured and plotted as a function of the frequency, Figure 1c shows that these angles are distributed in a narrow range of 121 to 130° (the detailed statistical results are described in Figure S1-S3 in the Supporting Information).

The typical morphology of such Ag NW joints is illustrated in the transmission electron microscopy (TEM) image in Figure 1c, where an angle of 125° is observed (Figure 1d). It is worth mentioning that the interior angle of the joint is sharp, because there is a large driving force for diffusion due to the high surface energy present at this location, while the outer surface has a larger radius or curved structure because the

P. Peng, Dr. L. Liu, Prof. A. P. Gerlich, Prof. A. Hu, Prof. Y. N. Zhou
Centre for Advanced Materials Joining
Department of Mechanical and Mechatronics Engineering
University of Waterloo
200 University Avenue West
Waterloo, ON, N2L 3G1, Canada
E-mail: p5peng@uwaterloo.cat; a2hu@uwaterloo.ca; nzhou@uwaterloo.ca
P. Peng, Prof. Y. N. Zhou
Waterloo Institute for Nanotechnology
University of Waterloo
200 University Avenue West
Waterloo, ON, N2L 3G1, Canada
Dr. L. Liu, Prof. Y. N. Zhou
Department of Mechanical Engineering
Tsinghua University, Beijing 100084, China

DOI: 10.1002/ppsc.201200099

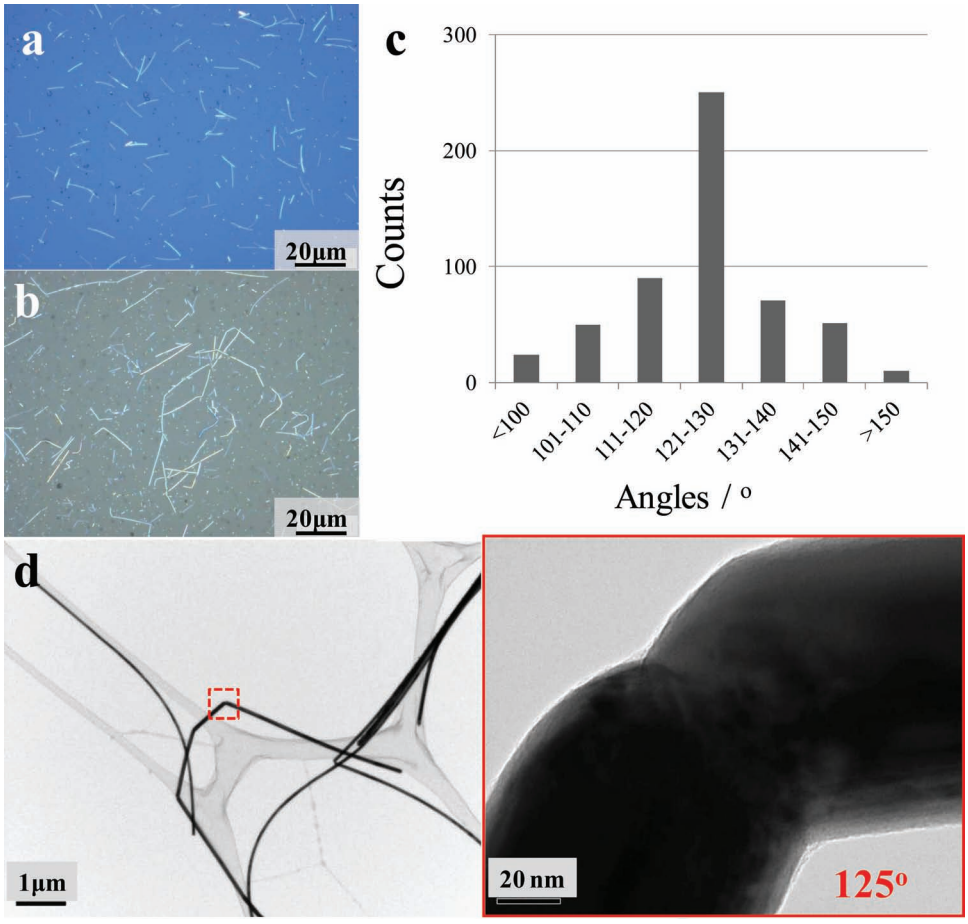

Figure 1. Optical microscopy images of a) pristine Ag NWs in EG and b) those washed with deionized water. Most of the Ag NWs were formed V-shaped or zig-zag Ag NWs with defining angles. c) Angle distribution of Ag NW joints. d) TEM images of typical Ag NW joints.

driving force for diffusion is low. This further supports the idea that these are joined, and not deformed wires because the outer surface of a deformed wire would be one continuous curve (not two curved surfaces as shown in Figure 1d). These structures differ from the previously reported V-shaped Ag NWs which formed due to twinned crystal plane induced growth and crystal lattice match induced fusion during polyol-thermal synthesis process.[23,24] It should be noted that these nanojunctions were formed at room temperature after the washing process without any heat input. Various washing processes, such as using acetone or ethanol, result in the same Ag NWs joints as those produced by washing with water (arrows indicated in the SEM image in Supporting Information Figure S4). These end-to-end Ag NW nanojunctions may be considered as having potential applications in the future nanoscale electronic circuits.[24]

For *fcc* metals, surface energy of different faces is uniform, and mainly depends on the variable density of atoms on each face.[25] In terms of silver, the surface atom density between the {100} and {111} planes is 1.2×10^{19} vs. 1.38×10^{19} atoms/m^2, respectively.[26] Consequently, the relative surface energies of the low-index crystallographic planes are $\gamma_{111} < \gamma_{100}$. Due to the stronger interaction between PVP and {100} facets than that between PVP and {111} facets resulting from the higher surface energy, it functions as a structure directing reagent on the surface of Ag nanomaterials during synthesis. Xia and co-workers identified that the end of Ag NW with five-fold cross-section is covered by {111} facets and with sides corresponding to {100} facets.[27] The weak interaction of PVP with the end facets of {111} leads to the higher chemical potential and reactivity on the ends, while the adsorption of PVP on side surfaces of {100} is very strong and results in complete coverage.[28] TEM images in **Figure 2**a,b support this notion and demonstrate that the organic shells have a 2.5 nm and 5 nm thickness on the ends and sides of as-synthesized Ag NW, respectively.

Once these Ag NWs intersect, this organic layer originating from the synthesis process could be presented at the interfaces of the nanowires and influence the interdiffusion of atoms to facilitate joining of Ag NWs without assistance of external energies, such as heat and pressure. Although the PVP absorbed on the surfaces of Ag NWs does not readily decompose at below 300 °C,[29,30] the majority of this organic compound would efficiently be removed during the process of washing with DI water as previously reported.[20] Figure 2c,d indicate the organic shell reduced to 0.5 nm on the end and 2 nm on the side of the Ag NWs after washing. Meanwhile, some areas on the ends of Ag NW were completely devoid of organic coating as indicated in

Particle
& Particle Systems Characterization
www.particle-journal.com

Materials Views
www.MaterialsViews.com

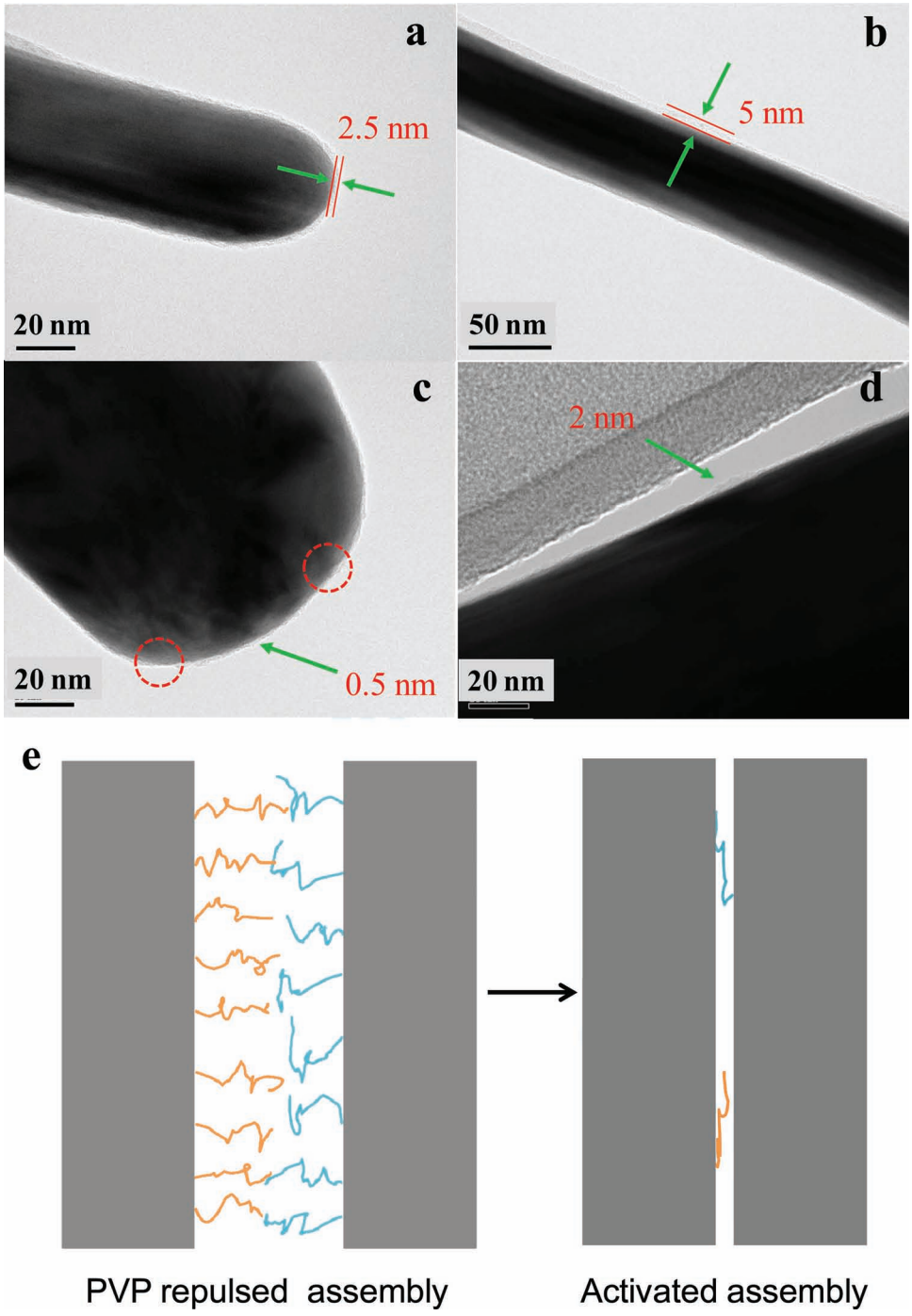

Figure 2. TEM images of the end (a) and side (b) of pristine Ag NW and c,d) washed Ag NWs. Amorphous layers of pristine Ag NW are 2.5 nm and 5 nm on the end and side. Those layers significantly reduced to 0.5 nm and 2 nm after washing, respectively. Some areas on the end of Ag NW were exposed without organic coatings as highlighted in the circles in (c). However, the breakage on the side of Ag NW is not significant in (d). e) Schematic of assembly of Ag NWs by modifying the surface of NWs with polymer chains grafts of different chain densities.

Figure 2c. These bare sites provide excellent interdiffusion channels between two NWs in contact in an end-to-end manner, which will promote spontaneous cold welding of Ag NWs due to the high driving force for surface diffusion at the nanoscale. It worth noting that external pressure during the centrifuge process might promote surface atom diffusion once two wires contacted. Even though the external force acted on each nanowire is very weak, the stress/pressure is quite high because of the small contact area at the nanowire interfaces between two ends in contact. However, the removal of PVP on the sides of Ag NW was not significant and the relatively thick organic layer (compared to the ends), would likely inhibit formation of

a T-shaped joint (end-to-side). This suggests that the ends of the Ag NW have been selectively activated for joining at room temperature and while keeping the rest of nanowire still protected.

It is worth noting that long polymer chains, PVPs in this case, graft on the surfaces of the nanowires and their presence could introduce repulsive secondary bonding forces between the two counterparts as demonstrated during Ag nanocube assembly.[31] These forces would lead to a gap on the order of few nanometers between the nanowires, impeding Ag atom diffusion as schematically shown in Figure 2e, since this gap is too large to facilitate the transfer of surface atoms and complete the diffusion process. The adsorption of polymer on the Ag surface also lowers the surface energy, leading to an increase in the activation energy of surface atoms.[32–34] Furthermore, the residual polymers present in the gap between the nanowires could block the diffusion channels.[35,36] However, if only a small fraction of the polymer material remains on the surface, the repulsive effect is reduced and the nanowire separation distance is much closer. Meanwhile, compared with large fraction, a small concentration of polymer could provide higher surface energy and lower activation energy of surface atoms to promote interdiffusion. Consequently, it promotes accelerated bonding between two surfaces and allows two Ag NWs to easily form metallic bonds at room temperature.

To understand the joining mechanism, HRTEM and SAED analysis were employed. **Figure 3** illustrates the TEM images and SAED patterns of one joint, where an angle of 126° is presented between the joined wires. The SAED pattern of upper wire shows the incident beam was on a [011] zone axis and the NW is twinned on the {111} plane with a 39° twining angle, see Figure 3b. Measuring from a [110] orientation, the angle between two (111) planes along twinning boundary is 70.53°,[37] yielding the complementary angle of two twinned planes is $180° - 2 \times 70.53° = 38.94°$, which is the observed twinning angle 39° through the diffraction patterns on the [011] zone axis. The measured angle between $(1\bar{1}\bar{1})$ and $(\bar{2}00)$ planes (or {111} and {100}) is 125°, which is in close agreement to the theoretical value of 125.26°. The diffraction pattern of bottom wire is illustrated in Figure **3**c. The length of index vectors shows that A/C = 1.95 and B/C = 1.65, indicating it is on the $[\bar{1}12]$ zone axis. The measured angle between $(\bar{2}\bar{2}0)$ and $(\bar{1}31)$ planes is 31° and in close agreement with the theoretical value of 31.48°, while angles between $(\bar{3}\bar{1}\bar{1})$ with $(\bar{1}\bar{3}1)$ and $(\bar{1}\bar{3}1)$ with $(1\bar{1}1)$ are 82° and 59°, respectively.

It is noted that there are also a group of weak diffraction spots indexed as [011] zone axis in Figure 3c. By rotating this set of spots by 55°, these are found to coincide with the [011] zone axis spots in Figure 3b. Moreover, the [110] direction has a 54.74° angle with [211] direction, i.e., an angle between $(\bar{1}10)$ and $(\bar{1}12)$. It is suggested that the two wires have the same orientations according to the diffraction patterns. In the other words, the bottom wire could be considered as rotating the top wire by 55° in-plane, which the angle is the difference between 180° and 55°, yielding the angle observed at the joints, 125°. Some slight deviation of the measured angle is due to the error of measurement and a result of viewing angle variation. The diffraction patterns for the jointed region are shown in Figure 3d, and it can be separated as two individual sets of spots, one from the top wire [011] zone axis and another for bottom wire $[\bar{1}12]$ zone axis. The HRTEM image of the joint taken from the interior angle illustrates two Ag NWs connected without any gaps, see Figure 3e. The lattice fringes indicate there is a 125° angle between (111) and (200) planes. Since its counterpart is not on the same zone axis, its lattice could not be revealed. Similar results were characterized in detail for another joint and shown in Figure S5 (Supporting Information).

The joints with smaller angles were also investigated to determine the orientation relationships of these joints, such as 115° as depicted in**Figure 4**a. Figure 4b,c show the diffraction patterns corresponding to the [011] and $[\bar{1}12]$/[011] zone axis as previous observation. Figure 4e displays the lattice fringes of the joint taken from exterior angle region, showing distances of the (111) planes from two Ag NWs were 2.4 Å and connected with a 10° misorientation. The dashed circle highlights the defect contrast due to this misorientation. This 10° misorientation has also appeared in diffraction patterns of the joint region

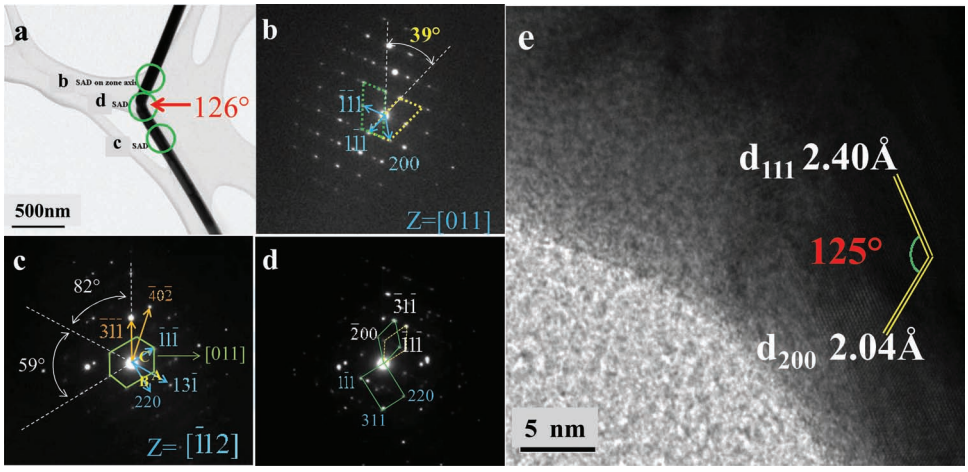

Figure 3. a) Ag NW joint with 126° angle: the SAED patterns on b) upper wire with [011] and c) bottom wire with $[\bar{1}12]$ zone axis, d) right the joint region. e) The HRTEM image of inner angle of the joint.

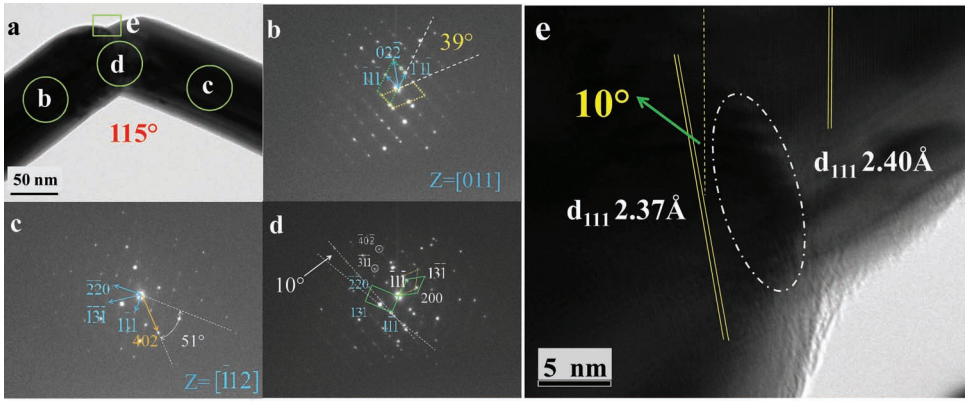

Figure 4. a) Ag NW joint with 115° angle. The SAED patterns on b) left wire with [011] and c) right wire with [$\bar{1}12$] zone axis, d) right the joint region. e) The HRTEM image of exterior angle of the joint, the (111) planes belong to two Ag NWs were matched with 10° misorientation. The dashed circle indicating the contrasts from defects because of the misorientation.

as shown in Figure 4d. As indicated in the angle measurements in Figure 1c, joints usually exhibit angles between 121–130°. Here, the measured angle of two Ag NWs 115° in Figure 4a corresponds to a misorientation angle 10° away from the 125° angle expected between the orientation relationship proposed here. Therefore, we suggest that the joints were formed by connecting two Ag NWs through lattice matching on (111) planes. Further, the misorientation accounts for the fluctuating angles of these joints, in the range of 115 to 135°, as the statistical results suggested (see Figure 1c). The interfaces within 10° misorientation are low angle grain boundaries, resulting from the grain boundary diffusion in conjunction with surface diffusion which dominates during joining. One could speculate that the two wires tend to be self-oriented to strive towards lattice matching on (111) planes during these diffusions.

Low stacking fault energy of silver materials promotes the crystal growth in nanosize, as a result of twins.[38] In the case of Ag NWs, the twin boundaries run along the entire wire, and the Ag NWs with five-fold cross-section could be considered as five highly orientated single Ag crystals ("triangular prisms", highly oriented nanoscale grains).[39] Each single prism is coherently twinned with another on the (111) plane and the end is covered by {111} facets. Joint formation has taken placed on these two {111} facets of the end of Ag NWs, see **Figure 5**a. Here, the joint was actually formed by the end of two single triangular prisms, and each of them was from the two joined wires. Since the extremity of the triangular prisms were (111) plane, the joint interface was $(111)_{NW1}//(111)_{NW2}$, or sometimes with a less than 10° mismatch. Therefore, a cleaned surface and identical lattice orientations are required for self-oriented joining of Ag nanowires at room temperature.

Considering the angle between {111} facets (on the end) and the axis of the NW is 54.74°, the self-oriented joined NWs will not be straight. If two NWs connect with alignment such that the centers of the pentagonal shapes (as labelled with red color region in Figure 5a) come into contact, then the angle between two joined NWs with same orientations would be 2 × 54.74° = 109.48°. This is an unfavorable angle as suggested in Figure 1c, and was not observed by TEM. Conversely, "center-to-edge" configuration of two NWs will allow the (111) lattices to easily match when the two end facets are not same size (two NWs with different diameters) and introduce more contact edge sites between two NWs, yielding much larger diffusion rate because the curvature of the NW decreases from the edge to the center, see Figure 5b. In this case, center-to-edge configuration could obtain around 50% higher energy edge sites than that of center-to-center configuration (with the as assumed angle configuration), as red dashed lines indicated in Figure 5b, leading to faster diffusion and nanojoining between center-to-edge aligned nanowire ends.

According to the lattice orientation relation of two Ag NWs, the atomic arrangement of the joint is reproduced in Figure 5c. The atomic arrangement indicates that the lattices of two joined "prisms" are well orientated and lattice matched. On each wire, the sides are terminated with a coherent twin boundary and free surface, respectively. We suggest that this joint creates a V-shaped prism with a monocrystalline structure. It is well accepted that the properties of crystals could be influenced by defects such as such as grain boundaries and free surfaces. Here, the same orientated V-shaped joint with two boundaries, a coherent twin boundary and free surface, may be a novel candidate to investigate the homogeneous transport properties in nonlinear Ag NWs, for example light/wave guidance and electronic transport of these joints. Furthermore, it has been shown that twin boundary within the NW for *fcc* structure could produce anomalous strength and brittle fracture under loading because the five twin boundaries in this type of NW were intersected with all of the possible slip systems in *fcc* structure and the motion of dislocations is restricted by the twinning boundaries.[40,41] Consequently, they are effectively grain boundary hardened materials[39] while these Ag NW joints with same orientations will be expected to gain good mechanical properties as that of original individual Ag NW.

In summary, Ag NW joints with similar angles are obtained through selectively activated surfaces contacting by simple washing processes using water, ethanol and acetone. Due to the weaker adsorption of PVP on {111} facets, it could be removed from the end of Ag NWs and make the {111} facets exposed

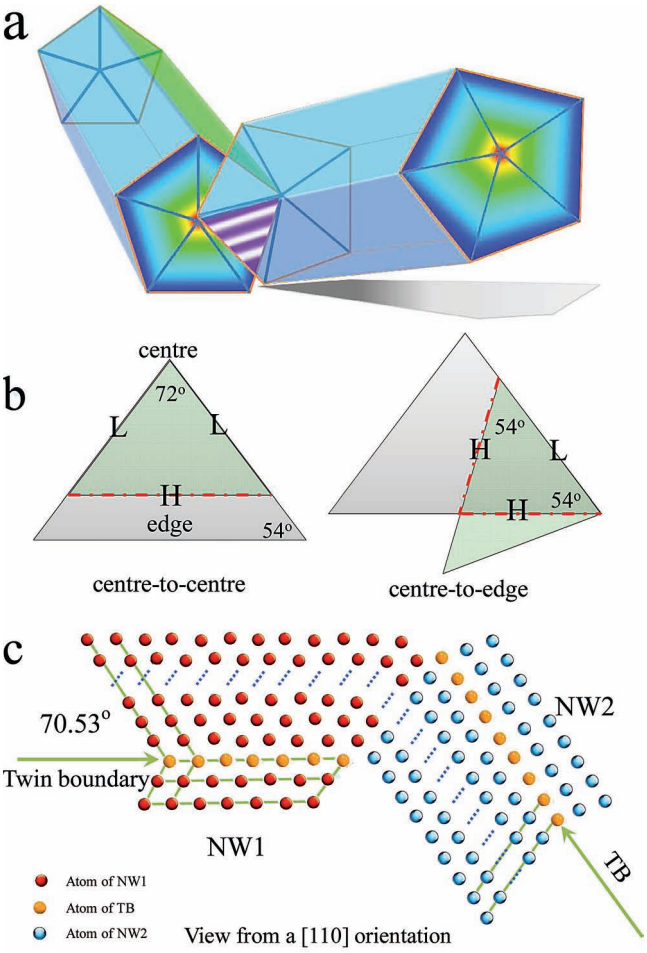

Figure 5. a) Schematic illustration of end-to-end Ag NW joint, the cross-section of Ag NW is five-folded. b) Two facets with different sizes attached via center-to-center and center-to-edge configurations, letters H and L denote high and low diffusion sites belonging to different locations of Ag NWs. c) The atomic arrangement of Ag NW join, when view from a [110] orientation that is on the coherent twin boundary with 70.53° angle of *fcc* Ag.

and activated for joining. Because of the high surface diffusion rate at nanoscale, much smaller separated gap and unimpeded diffusion channels by removal of PVP barrier layers, bared Ag NW ends could self-orientationally attach and join with its countparts with center-to-edge configuration by obtain high diffusion rate edge sites. This surface selective activation process for nanojoining of Ag NWs has the potential applications for building up nano-circuits. A monocrystalline V-shaped or *zig-zag* prism terminated by twin boundary and free surface is formed after self-oriented nanojoining. These welded regions have the similar crystal orientation and will be a novel structure for investigating the 1D transport properties in curved Ag NWs.

Experimental Section

Materials: Ag NWs were prepared in a polyol solution with polyvinylpyrrolidone (PVP) as a structure directing reagent using a method modified from the literature.[18,20–22] In this study, 330 mg polyvinylpyrrolidone or PVP ($(C6H9NO)_n$, K25, MW = 24 000, Alfa Aesar) and 12.5 mg silver chloride (AgCl, Alfa Aesar) were mixed with 40 mL ethylene glycol (EG, Fisher Chemical) and was heated to 170 °C. Then, 110 mg silver nitrate was dissolved in 10 mL ethylene glycol and added into the mixed solution while stirring vigorously and continuing the reaction conditions for 1 h.

Surface Activation Process: Three 10 mL as-synthesis Ag NW solutions were diluted to 50 mL using deionized (DI) water, ethanol and acetone, respectively. These diluted solutions sonicated for 5 min and centrifuged at 3000 rpm to remove the supernates and collect Ag NWs. Repeat this process twice.

Testing of V-Shaped Ag NWs: Optical microscopy (Olympus BX 51M, Japan) and field-emission scanning electron microscope (LEO 1530 FE-SEM) were used to study the microstructure of washed samples. Organic shells of Ag NW before and after washing and the diffraction pattern of Ag NWs were observed using high resolution transmission electron microscopy (HRTEM, JEOL 2010F).

Supporting Information

Supporting Information is available from the Wiley Online Library or from the author.

Acknowledgments

Support from the Canadian Research Chairs (CRC) program, the State Scholarship Fund of China (No. 2010640009), and National Sciences and Engineering Research Council (NSERC) is greatly acknowledged. L.L. would like to acknowledge partial support of this research by Tsinghua University Initiative Scientific Research Program (Grant No.2010THZ 02-1) and National Natural Science Foundation of China (Grant No. 51075232). The authors thank Mr. Fred Pearson from the Canadian Centre for Electron Microscopy, McMaster University for help with TEM operation.

Received: October 15, 2012
Revised: November 26, 2012

[1] Y. Lu, J. Y. Huang, C. Wang, S. Sun, J. Lou, *Nat. Nanotechnol.* **2010**, *5*, 218.
[2] Y. Peng, A. Cullis, B. Inkson, *Nano Lett.* **2008**, *9*, 91.
[3] Z. Gu, H. Ye, D. Smirnova, D. Small, D. Gracias, *Small* **2006**, *2*, 225.
[4] F. Gao, Z. Gu, *Nanotechnology* **2010**, *21*, 115604.
[5] L. Dong, X. Tao, L. Zhang, X. Zhang, B. J. Nelson, *Nano Lett.* **2007**, *7*, 58.
[6] H. Hirayama, Y. Kawamoto, H. Hayashi, K. Takayanagi, *Appl. Phys. Lett.* **2001**, *79*, 1169.
[7] C. Jin, K. Suenaga, S. Iijima, *Nat. Nanotechnol.* **2008**, *3*, 17.
[8] H. Tohmyoh, *J. Appl. Phys.* **2009**, *105*, 014907.
[9] Y. Wu, P. Yang, *Adv. Mater.* **2001**, *13*, 520.
[10] M. A. van Huis, *Nano Lett.* **2008**, *8*, 3959.
[11] V. Gopal, V. Radmilovic, C. Daraio, S. Jin, P. Yang, E. Stach, *Nano Lett.* **2004**, *4*, 2059.
[12] M. Wang, J. Wang, Q. Chen, L. Peng, *Adv. Funct. Mater.* **2005**, *15*, 1825.
[13] S. Xu, M. Tian, J. Wang, J. Xu, J. Redwing, M. Chan, *Small* **2005**, *1*, 1221.
[14] S. J. Kim, D. J. Jang, *Appl. Phys. Lett.* **2005**, *86*, 033112.
[15] F. Mafune, J. Kohno, Y. Takeda, T. Kondow, *J. Am. Chem. Soc.* **2003**, *125*, 1686.

[16] E. C. Garnett, W. Cai, J. J. Cha, F. Mahmood, S. T. Connor, M. G. Christoforo, Y. Cui, M. D. McGehee, M. L. Brongersma, *Nat. Mater.* **2012**, *11*, 241.
[17] X. Liu, J. Luo, J. Zhu, *Nano Lett.* **2006**, *6*, 408.
[18] Y. Gao, L. Song, P. Jiang, L. F. Liu, X. Q. Yan, Z. P. Zhou, D. F. Liu, J. X. Wang, H. J. Yuan, Z. X. Zhang, X. W. Zhao, X. Y. Dou, W. Y. Zhou, G. Wang, S. S. Xie, H. Y. Chen, J. Q. Li, *J. Cryst. Growth* **2005**, *276*, 606.
[19] Z. S. Pereira, E. Z. da Silva, *J. Phys. Chem. C* **2011**, *115*, 22870.
[20] P. Peng, A. Hu, H. Huang, A. P. Gerlich, B. Zhao, Y. Zhou, *J. Mater. Chem.* **2012**, *22*, 12997.
[21] P. Peng, A. Hu, B. Zhao, A. P. Gerlich, N. Y. Zhou, *J. Mater. Sci.* **2012**, *47*, 6801.
[22] Y. Sun, B. Gates, B. Mayers, Y. Xia, *Nano Lett.* **2002**, *2*, 165.
[23] X. C. Jiang, S. X. Xiong, Z. A. Tian, C. Y. Chen, W. M. Chen, A. B. Yu, *J. Phys. Chem. C* **2011**, *115*, 1800.
[24] D. Chen, L. Gao, *J. Cryst. Growth* **2004**, *264*, 216.
[25] C. Lofton, W. Sigmund, *Adv. Funct. Mater.* **2005**, *15*, 1197.
[26] B. Wiley, Y. Sun, B. Mayers, Y. Xia, *Chem. Eur. J.* **2005**, *11*, 454.
[27] Y. Sun, Y. Yin, B. T. Mayers, T. Herricks, Y. Xia, *Chem. Mater.* **2002**, *14*, 4736.
[28] Y. Sun, B. Mayers, T. Herricks, Y. Xia, *Nano Lett.* **2003**, *3*, 955.
[29] X. Yuan, C. Li, G. Guan, Y. Xiao, D. Zhang, *Polym. Degrad. Stabil.* **2008**, *93*, 466.
[30] M. Zheng, M. Gu, Y. Jin, G. Jin, *Mater. Sci. Eng., B* **2000**, *77*, 55.
[31] B. Gao, G. Arya, A. R. Tao, *Nat. Nanotechnol.* **2012**, *7*, 433.
[32] H. K. Christenson, *J. Phys. Chem.* **1993**, *97*, 12034.
[33] A. Kuznetsova, D. B. Mawhinney, V. Naumenko, J. T. Yates Jr, J. Liu, R. E. Smalley, *Chem. Phys. Lett.* **2000**, *321*, 292.
[34] C. T. Campbell, G. Ertl, H. Kuipers, J. Segner, *Surf. Sci.* **1981**, *107*, 220.
[35] W. Ludwig, A. Savara, R. J. Madix, S. Schauermann, H. J. Freund, *J. Phys. Chem. C* **2012**, *116*, 3539.
[36] J. M. Savéant, *J. Electroanal. Chem.* **1991**, *302*, 91.
[37] J. Reyes-Gasga, J. L. Elechiguerra, C. Liu, A. Camacho-Bragado, J. M. Montejano-Carrizales, M. J. Yacaman, *J. Cryst. Growth* **2006**, *286*, 162.
[38] U. Dahmen, C. Hetherington, V. Radmilovic, E. Johnson, S. Xiao, S. Luo, *Microsc. Microanal.* **2002**, *8*, 247.
[39] J. L. Elechiguerra, J. Reyes-Gasga, M. J. Yacaman, *J. Mater. Chem.* **2006**, *16*, 3906.
[40] J. Y. Wu, S. Nagao, J. Y. He, Z. L. Zhang, *Nano Lett.* **2011**, *14*, 5264.
[41] J. H. Seo, Y. Yoo, N. Y. Park, S. W. Yoon, H. Lee, S. Han, S. W. Lee, T. Y. Seong, S. C. Lee, K. B. Lee, P. R. Cha, H. S. Park, B. Kim, J. P. Ahn, *Nano Lett.* **2011**, *11*, 3499.